***Highlights**

> Strain compatibility and fault linkage is investigated in non-tabular relay zones.

> Faults link simultaneously at multiple points along overlapping tip lines.

> Mechanical layering controls the 3D shape of faults and hence linkage locations.

> Fault linkage controls the distribution of ramp rotation within a relay zone.

> Volumetric strains help maintain strain compatibility within a relay zone.

Strain compatibility and fault linkage in relay zones on normal faults

Jonathan J. Long*[1,2] and Jonathan Imber[1]

[1]Department of Earth Sciences, Durham University, Durham, UK

[2]Present address: Geospatial Research Ltd., Department of Earth Sciences, Durham University, Durham, UK

*Corresponding author: jonathan.long@durham.ac.uk

Abstract

Relay zones on normal faults are unlikely to have tabular geometries as depicted in idealised models. Rotation of a relay ramp between non-parallel and non-planar relay-bounding faults will inevitably lead to strain compatibility problems causing open gaps or overlaps within the relay zone. Linkage of relay-bounding faults does not evolve from a single branch point. Rather, linkage occurs at multiple points along the fault tip lines giving rise to initially discontinuous branch lines. Where linkage occurs along a discontinuous slip-aligned branch line, displacement at different levels within the relay zone is partitioned between variable amounts of ramp rotation and slip across the branch line. The linking fault propagates when strain compatibility can no longer be maintained by continuous deformation processes, such as thickening or thinning of incompetent layers within the relay ramp. Step-like changes in vertical displacement *vs*. distance (d-x) profiles on horizons containing apparently intact relay ramps are probably indicative of incipient breaching and can be used predict the presence of a slip-aligned branch line in the subsurface. Despite the complexity of the strain distribution within relay zones, the total vertical displacement across the relay remains geometrically coherent at all levels.

1. Introduction

The volume of rock within which faults overlap and transfer displacement is termed a relay ramp in map view and a relay zone in three-dimensions (3D). The bounding faults that define and enclose a relay zone are likely to be non-planar and non-parallel. Relay zones are therefore rarely, if ever, likely to have the simple tabular geometries depicted in the

idealised model (Fig. 1) proposed by Peacock and Sanderson (1994). Studies using 3D seismic reflection data or serial sections through relay zones on faults that cut unconsolidated sediments have refined this tabular relay zone model. These studies suggest that fault linkage occurs by the progressive replacement of fault tip lines by branch lines as two or more contemporaneous faults link (Walsh et al., 1999; Kristensen et al., 2008).

Non-tabular relay zones are a natural consequence of fault-surface propagation, bifurcation and linkage within layered, anisotropic host rocks (Schöpfer et al., 2006; Kristensen et al., 2008). Transfer of displacement between non-planar and non-parallel bounding faults inevitably results in strain compatibility problems within the relay zone with a tendency to open voids or cause overlaps between adjacent rock volumes (Walsh and Watterson, 1991). Such problems are particularly acute at sites of fault linkage, where fault orientations are likely to vary both along strike and down dip (e.g. Walsh et al., 1999; Davatzes et al., 2005; Bonson et al., 2007). The intensity and type of strain within and around relay zones must vary spatially and temporally to maintain strain compatibility. Despite the potential for heterogeneous deformation, sites of fault linkage are widely inferred to be geometrically and kinematically coherent, such that fault-related strains maintained regular and systematic distributions throughout their evolution in both space and time (Walsh and Watterson, 1991; Childs et al., 1995; Walsh et al., 2003; Long and Imber, 2010). A key question, therefore, is how does the rock volume containing the relay zone deform to maintain strain compatibility and kinematic coherence? This information is of practical importance given that relay zone deformation and fault linkage strongly influence the hydraulic properties of fault zones and, in the case of seismogenic faults, the dimensions of potential earthquake ruptures.

The aim of this study is to investigate how strains are accommodated, and how fault linkage develops within non-tabular relay zones on normal faults that cut layered sedimentary sequences. We present a detailed study of a relay zone imaged by a high quality 3D seismic reflection dataset from the Laminaria High, northern Bonaparte basin, on the NW continental margin of Australia (Fig. 2a). This relay zone is characterised by linkage along branch lines that are aligned sub-parallel to the fault slip vector ("slip-aligned fault linkage"). The novelty is that we apply the "fault-normal rotation" method developed by Long & Imber (2010) to map and quantify both the continuous *and* discontinuous components of deformation at multiple structural levels. In particular, we use apparent dips of deformed seismic reflectors to map and analyse fault-normal shear strains within the *volume* containing the studied fault array. This approach permits a more complete analysis of relay-zone deformation than traditional methods that only consider the throws on seismically-imaged faults, or that "collapse" the continuous and discontinuous components of

deformation into a single throw value on the fault plane, thereby losing the spatial distribution of deformation.

We have ground-truthed the processes inferred from our subsurface interpretations against observations of a well-exposed relay zone on a normal fault array that crops out at Lilstock, UK. Our results show that relay-bounding faults that cut layered sedimentary sequences link along multiple branch lines or branch points simultaneously, resulting in complex strain distributions within the relay zone. Relay ramps may display highly variable magnitudes and distributions of dip towards the mutual hanging wall at different levels within the relay zone. Despite this variability, our findings demonstrate conclusively that the total vertical displacements across the studied relay zones resemble that of a single fault at all levels and, presumably, all stages of fault linkage evolution, implying that the relay zones are geometrically and kinematically coherent.

2. Method: analysis of fault-normal rotations in 3D seismic reflection data

We mapped 14 seismic reflectors that were deformed and offset by a fault array on the Laminaria High (H1 = seabed reflector; H14 = near top Eocene reflector; Figs. 3 and 4). Care was taken such that the horizon picks follow the seismic reflections precisely to capture small-scale undulations that arise from deformation within and around the relay zones. We then created 14 high-resolution "trimesh" surfaces (3D triangle meshes) from the raw horizon interpretations to calculate the apparent dip of each horizon along transect lines orientated at 90 degrees to the average strike of the fault array. Transect lines were spaced at a 25 m horizontal interval. The same transect lines were used to sample the apparent dips on every horizon in order to constrain the variation in apparent dip within the volume containing the fault array. Horizon trimeshes were then contoured for apparent dip (e.g., Figs. 5 and 6).

We use the term "fault-normal rotation" to describe apparent dips sampled in this way. Fault-normal rotation is equivalent to "fault-normal shear" defined by Huggins et al., (1995). Fault-normal rotation characterises both the continuous and discontinuous components deformation at the scale of observation. Fault-normal rotation therefore quantifies the *total vertical displacement* for seismically-imaged fault arrays (See Long and Imber, 2010; Long, 2011, for details). Regions of fault-related deformation can be identified on the contoured horizon maps as elongate bands in which the apparent dip deviates from the regional dip of

100 the horizon (e.g., Figs. 5 and 6). Abrupt changes in apparent dip caused by miss-ties due to
101 mismatches between seismic lines or interpretation errors, and/or fault-normal rotation not
102 directly associated with the studied fault array due to far-field deformation caused by slip
103 on neighbouring fault arrays, and/or the presence of down-cutting sedimentary channels,
104 were removed by visual inspection and were excluded from further analysis (See Long and
105 Imber, 2010, for details).

106 An advantage of the fault-normal rotation method is that we can interpret fault-linkage
107 geometries on both vertical seismic sections (See Walsh et al., 1999) *and* contoured horizon
108 maps. The former are more suitable for identifying sub-horizontal branch lines and the
109 latter sub-vertical branch-lines. Fault linkage is inferred on fault-normal rotation maps
110 where two or more laterally continuous bands of high apparent dip coalesce (Long, 2011).
111 Fault linkage is confirmed by inspecting vertical displacement *vs.* distance (d-x) profiles.
112 Abrupt changes in vertical displacement are indicative of fault linkage (Maerten et al., 1999;
113 Wyrick et al., 2011) and arise because displacement is transferred between faults at a
114 branch point or branch line. Parts of the relay-bounding fault surfaces become inactive,
115 giving rise to low displacement, "relict" fault tips (Ferrill et al., 1999).

116 Two potential sources of error or geological uncertainty arise from fault-normal rotation
117 maps and associated d-x profiles with respect to determining deformation magnitude. First,
118 the fixed orientation of the transect lines will lead to under-estimation of total vertical
119 displacement where fault strike is locally sub-parallel to the transect lines (Long and Imber,
120 2010). Such effects are particularly important where linking faults are highly oblique to the
121 average strike of the fault array. Careful inspection of seismic sections in conjunction with
122 the contoured horizon maps minimises the effects of these sampling errors. Second, the
123 maps and d-x profiles record the *finite*, not incremental fault-normal shear. Given that a
124 component of the observed fault-normal rotation is likely to have developed in the rock
125 volume ahead of the fault tips during *propagation* of the relay-bounding faults, the
126 measured rotation incorporates the effect of deformation prior to and after the propagation
127 of the tip through the sample position. On the Laminaria High, the studied relay-bounding
128 faults were active during the deposition of the mapped H1 to H4 interval (Fig. 3; Long, 2011).
129 It is therefore possible to make a qualitative assessment of the strains due to fault
130 propagation and relay zone evolution by examining structures at different levels within this
131 growth sequence.

132

3. Geological background: Laminaria High, Bonaparte Basin, NW Australia

The Laminaria High is located within the Northern Bonaparte basin on the NW continental margin of Australia (Whittam et al., 1996; De Ruig et al., 2000). Faults in the top 2.5 km of sediment were analysed using a well-calibrated 3D seismic reflection dataset (Fig. 3), which covers the Laminaria High and has an area of approximately 760 km^2. It was collected in 1995 in an E-W direction with asymmetric binning (12.5 x 25 m), and is a time-migrated volume. Fourteen horizons were interpreted on bright, laterally continuous reflections (Fig. 3) from the top 1.8 seconds (ca. 2.5 km) two-way travel time (TWT). Regional dips of stratigraphic reflectors are mainly sub-horizontal, or gently toward the northeast (Fig. 2).

Wireline logs from a borehole on the Laminaria High show that the density of the carbonate-dominated sedimentary sequence does not vary greatly with depth, apart from around horizon H9, which is characterised by elevated acoustic impedance and a peak in corrected density (Fig. 3c). Velocity data from a nearby well was used to depth convert a seismic section (Fig. 3b). The velocity profile is consistent for a uniform overburden with negligible lateral velocity variations. Therefore, the depth conversion process had a minimal effect on the overall geometries, producing little change in fault geometries between the depth and time sections. Consequently, the time-migrated volume was used to analyse the distribution of fault-normal rotation for the studied relay zones.

Faults in the study area initiated within the Tertiary overburden during the Mio-Pliocene, and propagated downward toward reactivated east-west trending Mesozoic faults (De Ruig et al., 2000). Across-fault sequence expansion suggests that the mapped H1 to H4 (Plio-Quaternary) interval was deposited during slip on the studied fault array (Figs. 2 and 3; see Long 2011 for details). All mapped faults show apparent normal offsets. Syn-tectonic mass transport complexes (MTC) and channel features are present throughout the area. Analysis of piercing points where MTCs and channels are cut by faults implies purely dip-slip movement, which is a result also noted by De Ruig and others (2000: their Fig. 11).

4. Slip-aligned fault linkage, Laminaria High

4.1. Relay zone geometry

In cross-section, the traces of the relay-bounding faults, F3 and F2 are sub-parallel and decrease in dip with depth (Fig. 4a). This decrease in fault dip gives rise to a non-tabular

relay zone. The total throw across faults F2 and F3 is about 60 ms TWT. The horizons within the ramp dip toward the mutual hanging wall, as observed in many other relay zones (Huggins et al., 1995). The average thickness between pre-faulting horizons H4 and H9 outside of the relay zone is 241 ms TWT, whereas the thickness between the same markers within the relay zone is lower at 235 ms TWT. The possible cause of this thickness change within the relay zone is discussed in section 6. No slip-normal branch line is observed at the base of the relay zone on this cross-section. Minor faults occur in the volume adjacent to the relay zone with an increase in the density of secondary faults on horizon H9 (Fig. 4a: dashed lines). The upper tip points of F2 and F3 both terminate within the growth sequence. The upper tip point of F2 lies above horizon H2, whereas F3 stops midway between H3 and H2. This observation suggests that at the location of the cross-section, F2 continued to move after F3, which is consistent with the inference that F3 is a relict splay.

In map view, the separation (i.e. the perpendicular distance) between the footwall (F3) and hanging wall (F2) faults to the R1 relay ramp is approximately 100 m (Fig. 4b). A fault enhancement seismic attribute ("ant-tracking"; Pedersen et al., 2005) has been applied to horizon H8. This attribute highlights two linear features that coalesce at the north-east end of the ramp. This observation suggests that the faults are linked at a branch point on horizon H8 (Fig. 4b). The combined observations from map and cross-section views are consistent with the idea that F2 is now the through-going fault surface, formed when F2 and F3 linked at the north-east end of the ramp along a slip-aligned branch line. It is at this point that most published studies into fault linkage geometry would stop, but we continue our analysis and present detailed observations of fault interaction and linkage based on our analysis of fault-normal rotation.

4.2. Spatial distribution of fault-normal rotation

We analysed the fault-normal rotation on six representative horizons that contain structures associated with the R1 relay zone (Fig. 5). The pattern of fault-normal rotation is different for each horizon, with a marked change in the distribution of fault-normal rotation occurring on horizons H8 and H9 (Figs. 4 and 5). On horizon H2, the relay-bounding faults F2 and F3 overlap by approximately 135 m and the relay ramp dips toward the mutual hanging wall with between 4°and 6° apparent dip. On horizon H4, faults F2 and F3 overlap by 625 m. The relay ramp again dips toward the mutual hanging wall, but the magnitude of apparent dip varies between 2° and 8°. The ramp is open at both ends but the separation distance between the F3 and F2 decreases to less than 100 m in the vicinity of transect line 550 (Fig. 5).

On horizon H7, the band of fault-normal rotation associated with F2 coalesces with that associated with F3 at a branch point adjacent to transect line 545. This pattern is consistent with observations of the fault enhancement seismic attribute seen in Figure 4b. The lateral tip of F3 is characterised by progressively decreasing magnitudes of fault-normal rotation between transect lines 545 to 530. In contrast, the magnitude of fault-normal rotation remains consistently high along the length of the adjacent F2 structure. This observation supports our earlier inference that F2 is now the through-going structure, with the low-displacement tip of F3 being a relict splay. On H7, the relay ramp again dips toward the mutual hanging wall, but the apparent dips are generally smaller at 0° and 2° than those observed on H4.

The relay-ramp geometries on horizon H8 are similar to those on H7 with the north-eastern tip of fault F2 coalescing with F3 at a branch point near transect line 545 (Fig. 5). The relatively small value of fault-normal rotation adjacent to the branch point is an artefact caused by the strike of the linking fault being approximately parallel to the transect line orientation. Apparent dips within the relay ramp are patchy and generally of small magnitude. A ca. 1 km wide zone comprising elongate bands of small to moderate fault-normal rotation exists to either side of the R1 relay ramp, a feature that is also observed on horizon H9, and adjacent to fault arrays on laterally equivalent horizons elsewhere on the Laminaria High (Long 2011).

On horizon H9, the two bands of large fault-normal rotation associated with the relay-bounding faults, F2 and F3, do not coalesce at a branch point. This pattern is most simply interpreted as representing an open relay ramp. The internal distribution of fault-normal rotation in the relay ramp more closely resembles that on horizon H4 than the overlying horizon H8 with locally large magnitudes of apparent dip toward the mutual hanging wall (Fig. 5). Finally, horizon H12 is characterised by a continuous northeast-southwest trending band of high fault-normal rotation. This band is the down-dip continuation of both the F2 and F3 faults. No branch point or slip-normal branch lines are directly imaged between H9 and H12 (Figs. 4 and 5), although a branch point or slip-normal branch line must exist where faults F2 and F3 merge into the continuous fault trace observed on horizon H12.

4.3. Vertical displacement *vs.* distance (d-x) profiles

The vertical displacement *vs.* distance (d-x) profiles for the R1 relay show the throws on faults F2 and F3 (Fig. 5: solid lines), the vertical displacement due to continuous fault-normal rotation on either side of the mapped faults (Fig. 5: dotted lines), and the total vertical

displacement (Fig. 5: dashed lines). Lateral fault tips are inferred at the points where the total vertical displacement associated with F2 and F3 decreases to zero. Fault lengths determined in this way are, on average, a few hundred metres longer than fault lengths determined by the traditional method of extrapolating seismically-resolvable fault throws (Long & Imber 2011). The smoothly varying total vertical displacement profile for R1 resembles that of a single, continuous fault on all horizons (Fig. 5).

On horizon H2, the displacement on F2 and F3 decreases smoothly towards the lateral fault tips, with greater displacement gradients within the fault overlap zone (Fig. 5). In contrast, the displacement on F3 decreases abruptly to the southwest of the branch point between F2 and F3 on horizons H7 and H8 in the vicinity of transect line 545 (Fig. 5: arrows). These observations are consistent with our previous interpretation of fault linkage, such that part of F3 located to the south-west of the branch point being a relict fault tip. A small, but noticeable step-like decrease in displacement on F3 is also observed on horizons H4 and H9, in the vicinity of transect line 545, which is directly above and below the branch points interpreted on H7 and H8 (Fig. 5: arrows).

The broad zone of deformation observed on horizons H8 and H9 clearly contributes to the geometrically coherent total vertical displacement profiles associated with H8 and H9. This zone of continuous deformation extends beyond the R1 fault overlap (Fig. 5) and surrounds the fault array that includes the relay-bounding segments F2 and F3 outside the immediate study area (see Fig. 2b; Long 2011). These observations suggest that the zone of elevated fault-normal rotation did not initiate to accommodate strains within any single relay zone. Instead, we postulate that it originated as a regional flexure during propagation of the fault array, perhaps because horizons H8 and H9 acted as temporary barriers to fault propagation.

4.4. Three-dimensional structure

The three-dimensional structure of the R1 relay can be interpreted from a vertical “stack” of horizon maps contoured for fault-normal rotation. Fault tip and branch line geometries can be extrapolated between mapped horizons to highlight the fault-surface geometries (Fig. 6). It is apparent from Figure 6 that despite its relatively simple cross-sectional geometry (Fig. 4a), the R1 relay zone is non-tabular in form. The relay zone geometry varies from an open or intact ramp on H2 to H4, to a breached ramp on H7 to H8. Here, F2 and F3 link along a slip-aligned branch line. The relay zone is again open on H9, and terminates downward at a branch point or slip-normal branch line between H9 and H12 (Fig. 6). In detail, each horizon is characterised by variable amounts of ramp rotation toward the mutual hanging wall.

Horizons H2, H4 and H9 display relatively large rotations, compared to horizons H7 and H8. Published models of 3D fault linkage would predict a continuous branch line propagating outwards from the branch point (Walsh et al., 1999). Our observations suggest that simultaneous linkage at multiple branch lines or branch points along overlapping fault tip lines is possible. This 3D structure, with a discontinuous slip-aligned branch line and variable ramp dips also implies strain compatibility or space problems are likely to develop within the relay zone. However, the limited vertical and horizontal resolution of the seismic reflection data makes it impossible to determine the mechanisms by which strain compatibility is maintained within the R1 relay zone. We therefore use an exposed relay zone at Lilstock as a natural proxy with greater available resolution to investigate how strain compatibility is achieved in relays with slip-aligned branch lines.

5. Slip-aligned fault linkage, Lilstock

Our outcrop example is located on a wave-cut platform in northern Somerset, UK (Long 2011). The relay-bounding faults cut and offset Lower Jurassic rocks comprised of moderately dipping, interbedded limestones and shales (Peacock and Sanderson, 1991, 1994; Long, 2011). Limestone beds typically range from 5 cm to 1 m in thickness, whereas shale beds are between 5 cm and 5 m thick. The fault array trends east-west and the relay-bounding faults display normal dip-slip displacements, with no signs of strike-slip or reverse reactivation. The faults are believed to have nucleated within the more competent limestone beds (Peacock and Sanderson, 1991, 1992). The relay-bounding faults have a horizontal separation of 90 cm across the relay ramp, and a combined maximum offset of 68 cm. The relay zone was breached by the propagation of the footwall fault across the top of the ramp. Crucially, a slip-aligned branch line is visible on the exposed fault surface (Fig. 7).

A longitudinal profile through the relay zone is exposed in front of the footwall fault (Fig. 7). Here, the relay zone comprises three limestone beds (1 = youngest; 3 = oldest; the sequence has not been inverted) that define a westward dipping relay ramp. The limestone beds are interbedded with shale layers of variable thickness (S1 = youngest; S2 = oldest; Fig. 7). Limestone beds 2 and 3, east of the branch line, protrude outwards toward the camera position and the offsets in the photo appear foreshortened. The measurements given below were taken directly from the outcrop and from detailed terrestrial laser scan data (Long 2011). Limestone bed 1 is 21 cm thick, and is offset by 9 cm across the slip-aligned branch line. Within the relay zone, the bed dips at 14° towards 213° adjacent to the branch line and at 09° towards 211° at a point 1 m to the west of the branch line. Limestone bed 2 is 8.5 cm

thick, and is offset by 3.5 cm across the branch line. It dips at 55° towards 216° adjacent to the branch line and 13° towards 214° at a point 1 m to the west of the branch line. Finally, limestone bed 3 is also 8.5 cm thick, and is offset by 2.1 cm across the branch line. Its dip is 25° towards 218° adjacent to the branch line and 14° towards 213° at a point 1 m to the west (Fig. 7). The limestone beds within the relay zone are therefore not parallel adjacent to the slip-aligned branch line (Fig. 7).

Moving west away from the slip-aligned branch line, limestone beds 2 and 3 become parallel with bed 1. At horizontal distances greater than 1 m from the branch line the shale layer S1 is 17 cm thick and S2 is 24 cm thick. Immediately west of the slip-aligned branch line S1 is 10 cm thick and S2 is 18 cm thick. The shale beds have changed in thickness, to accommodate the changing dips of the competent limestone beds. The total vertical offsets of beds 2 (16.9 cm) and 3 (16.7 cm; estimated from typical bed thickness of S2 away from the branch line) measured between locations A within the footwall and A' within the relay zone are approximately equal to the total vertical offset of bed 1 (16.7 cm) measured between the same locations (Fig. 7). Thus, displacement is conserved at all levels within the relay zone, but is partitioned between variable amounts of slip across the branch line and rotation of the limestone beds. Strain compatibility is maintained by movement of the incompetent shale layers.

6. Discussion

6.1. Influence of mechanical layering

Mechanical layering influences fault-tip propagation (Peacock and Sanderson, 1992; McGrath and Davison, 1995; Childs et al., 1996; Ferrill and Morris, 2003; Crider and Peacock, 2004). Propagation is more rapid in competent layers (e.g. carbonates) than in incompetent layers (e.g. shales) (Schöpfer et al., 2006; their Fig. 13). The thicker, more competent limestone bed 1 at Lilstock may have facilitated rapid fault propagation, allowing linkage at an early stage during relay zone evolution. In contrast, the relay ramp on limestone beds 2 and 3 would have remained intact for longer. Following linkage, bed 1 preferentially accommodated offset by increased slip on the breaching fault, whereas beds 2 and 3 continued to accommodate displacement by rotation of the beds in the relay ramp. Differential rotations were facilitated by thickness changes within the surrounding shale beds. These findings are consistent with the results of three-dimensional distinct element method models of relay growth and breaching, which show that the dips of open relay

ramps are higher than the dips of breached relay ramps at different levels within the same partially-breached relay zone (Imber et al., 2004).

Observations of variable ramp dip and displacement across the slip-aligned branch line in Lilstock (Fig. 7) suggest that the high values of fault-normal rotation observed on open relay ramps in the partially-breached R1 relay ramp on the Laminaria High (Fig. 5) reflect variable partitioning of displacement between slip across the branch line and reflector rotation at different levels within the relay zone. Localised peaks in gamma ray intensity obtained from well logs in hydrocarbon wells on the Laminaria High (e.g. Fig. 3c) suggest that interbedded shales may be present with the carbonate-dominated Neogene sequence. Strain compatibility may have been achieved in R1 by thickening and thinning of interbedded shale layers (e.g. Fig. 3) and/or tectonic dissolution of the competent carbonate beds. This inference of tectonic dissolution is consistent with the decreased thickness of the pre-faulting H4 to H9 sequence within the R1 relay zone.

To summarise, spatial variations in strain intensity appear to be a natural consequence of fault linkage, and are to be expected even in relatively simple relay zones (such as R1) that are enclosed by sub-planar bounding faults and where the branch line is aligned parallel to the slip direction. Deformation processes at a scale smaller than observed with the seismic reflection imagery produce continuous structure geometries at the seismic scale that maintain strain compatibility throughout the relay zone. The question then arises what happens when processes that create the thickness changes within incompetent beds can no longer accommodate differential rotations within the relay zone?

6.2. Strain compatibility and linkage along slip-aligned branch lines

Breached and open ramps coexist at different depths within partially-breached relay zones, such as R1. Where the ramp is breached, slip occurs at the branch line on the through-going fault surface, whereas open relay ramps continue to rotate, increasing the magnitude of fault-normal rotation. Vertical displacement *vs.* distance (d-x) profiles for horizons with open relay ramps show a small, but abrupt, drop in displacement on one of the relay-bounding faults that occurs directly above or below the site of fault linkage on adjacent horizons containing a linked relay ramp (Fig. 5: horizon H9). In three-dimensions, this displacement reduction occurs on the fault surface that contains the relict tip on the under- (or over-) lying horizon (Fig. 8). We interpret these observations to mean that the relay-bounding faults adjacent to these ramps that appear to be intact at the seismic scale are undergoing incipient linkage.

The presence of relict tips on horizons containing breached relay ramps may lead to restricted displacement on the *entire* fault segment (Fig. 8). Such abrupt variations in fault displacement on horizons containing apparently intact relay ramps may be necessary to maintain strain compatibility within partially-breached relay zones, where processes such as thickening or thinning of incompetent layers and/or tectonic compaction or dissolution are insufficient to accommodate large differential ramp rotations at different levels within the relay zone. Linkage of the relay-bounding faults along slip-aligned branch lines is therefore likely to be controlled by the ability of the relay zone to deform internally. This hypothesis suggests that for any given separation distance, relay zones between faults that cut low net to gross sequences and hence, have a large proportion of incompetent shale layers, may remain intact for greater displacements than those in high net to gross sequences, which contain only thin incompetent shale layers. A corollary of our findings is that the shapes of d-x profiles (i.e. the presence or absence of a "stepped" displacement profile) should be usable to predict whether apparently open relays zone exposed at the surface are breached along slip-aligned branch lines in the subsurface (Fig. 8). This result is similar to that of Soliva et al. (2008) who inferred slip-normal fault linkage from the asymmetric displacement distribution on overlapping faults.

The maximum possible size of an earthquake rupture is determined by the size of the fault surface (e.g. Schwartz and Coppersmith, 1984; Wesnousky, 1986; Machette et al., 1991; Sieh et al., 1993; Amato et al., 1998; Ferrill et al., 1999; Soliva et al., 2008), which is why understanding fault linkage geometries in 3D is vital to assessing the size of potential earthquakes. A relay zone that is open at the earth's surface might be linked along a slip-aligned branch line at depth, thus increasing the size of the potential rupture plane and the resultant earthquakes (Soliva et al., 2008). When 3D sub-surface data are not available, the shape of a d-x profile could be used to predict whether a relay zone is breached along a slip-aligned branch line in the subsurface. Thus, the ability to predict fault linkage at depth using fault throw and fault-normal rotation measurements collected from outcrops or remote-sensing data could be an important refinement in seismic hazard mapping.

7. Conclusions

1. Analysis of the total vertical displacement that combines fault throw and the vertical component of continuous deformation across a fault array imaged by a high-resolution three-dimensional seismic reflection dataset confirm that relay zones are geometrically and

kinematically coherent through all levels, regardless of the deformation partitioning within the relay zone.

2. Linkage of the relay-bounding faults does not evolve exclusively from a single branch point, but develops at multiple branch lines and/or branch points along overlapping fault tip lines. As a result, branch lines are likely to be segmented and discontinuous, at least during the initial stages of fault linkage.

3. Apparently intact or unbreached relay ramps display larger dips towards the mutual hanging wall than breached relay ramps at different levels within the same partially-breached relay zone.

4. Field observations from a well-exposed breached relay zone, in an interbedded limestone-shale sequence, show that the amount of slip and bed rotation on the competent limestone layers varies with lithology and bed thickness within a relay zone. Strain compatibility is achieved by thickening and thinning of incompetent shale layers.

5. Vertical displacement *vs*. distance (d-x) profiles across a partially-breached relay zone show step-like drops in displacement at slip-aligned branch lines, consistent with the results of previous studies. Smaller step-like drops in displacement are also observed on under- and over-lying horizons, directly adjacent to the mapped location of fault linkage.

6. Step-like d-x profiles for horizons containing apparently intact relay ramps represent a state of incipient breaching and linkage of the relay-bounding faults along slip-aligned branch lines. Further propagation of the breaching fault is inferred to take place when continuous deformation processes at the scale of observation can no longer maintain strain compatibility within the relay zone by differential bed rotations.

Acknowledgements

We are grateful for the constructive reviews provided by David A. Ferrill and Brent Couzens-Schultz, and to Wayne Bailey for introducing us to the Laminaria High dataset. Bill Dunne provided helpful editorial guidance. We thank Badley Geoscience Ltd. for providing the TrapTester software used in this study, and Brett Freeman for coding the algorithm that enabled us to extract fault-normal rotation data from TrapTester horizon meshes. JJL was funded by a NERC Open CASE PhD studentship with BG Group (NE/F006586/1) and is grateful for being given the opportunity to finish writing the manuscript by Geospatial Research Ltd.; JI is funded by Statoil (UK) Ltd.

Figure captions

Fig. 1. A conceptual 3D diagram of a relay zone. Ramp rotations towards the mutual hanging wall are depicted to be constant on each horizon, despite the progression in fault linkage from an open to linked and finally breached relay ramp with increasing depth. A relict fault tip is formed when the ramp is breached by a through-going master fault. Modified from Peacock & Sanderson (1994).

Fig. 2. (a) Geological setting and Late Jurassic structural elements of the NW Australian shelf. The location of the Laminaria3D seismic survey is annotated. (b) Time structure map of horizon H8 (Fig. 3) contoured in milliseconds two-way travel time (ms TWT). The location of the R1 relay zone is highlighted, along with seismic section locations. The Laminaria 1 well is located about 4 km south of the mapped area along the lateral continuation of the seismic line location labelled “Fig. 3”. Fault polygons can be identified by closely spaced contours. (c) An isochron map for the H2 to H4 growth sequence, where horizon H4 is the base of the syn-faulting sedimentary sequence (Fig. 3). Abrupt changes in sequence thickness delimit the location of active faults at the time of deposition. All fault segments on the NE-SW trending fault-array were active during the same time. The studied R1 relay zone is labelled.

Fig. 3. (a) Lithostratigraphic column for the Laminaria High based on the Laminaria 1 well (10 37' 40.563" S and 126 01' 42.051" E) and regional studies by De Ruig et al. (2000). (b) Depth-converted vertical seismic reflection profile that intersects the Laminaria 1 well. The well location is marked by an arrow-head and the fourteen interpreted horizons are shown. (c) Log curves from the Laminaria 1 well showing corrected density (DRHO; right) and gamma ray (GR; left).

Fig. 4. (a) Vertical seismic profile through the R1 relay zone (Fig. 2). (b) Map showing a fault enhancement seismic attribute for horizon H8, contoured for two-way travel time (TWT). The thin black line marks the location of the seismic profile (a).

Fig. 5. Horizon maps and vertical displacement *vs*. distance (d-x) profiles for six horizons that intersect the R1 relay zone (Fig. 4). Each map is contoured for fault-normal rotation (grey scale) and two-way travel time (TWT; solid lines). The transect line numbers for each set of maps and profiles are given at the bottom. The locations of transect lines on the maps and profiles are shown by the grey vertical lines. The black arrows indicate the location of inflection in the d-x profiles and thus the possible location of fault linkage.

Fig. 6. Composite 3D view of the R1 relay zone showing the distribution of fault-normal rotation at different depths. Interpreted fault traces are shown by white dashed lines. Horizons H7 and H8 are omitted for clarity but the positions of the fault traces on these horizons are shown schematically by the thin black lines. Solid black lines indicate the location of the interpreted fault-tip lines. Dashed lines indicate where a fault-tip line is hidden by a fault surface in the foreground. Bold lines indicate branch lines and the branch point is circled. There is a gap in the branch line from H9 until the branch point (circle) above H12.

Fig. 7. Lilstock relay ramp, Somerset, UK (488529, 5672747, UTM 30N). (a) An interpreted field photo showing a longitudinal profile through a relay zone. The exposed slip-aligned branch line (dashed white line) links the footwall fault (FWF) and hanging wall fault (HWF). Sketch lines follow bedding surfaces and highlight the lateral changes in bed dip. White arrows indicate offset and sense of movement on exposed fault surfaces. Individual limestone and shale beds are numbered. A and A' are the measurement locations described in the text. View looking south. 40cm tape measure in centre of view for scale. (b) Map view of a textured point cloud produced using a terrestrial laser scanner, depicting the geometries of the overlapping faults. The majority of the map consists of the top of limestone bed 1. The location of the branch line is at the east end of the relay ramp, highlighted with a white box.

Fig. 8. Schematic model illustrating the effect of slip-aligned fault linkage on open relay ramps within the same relay zone. (a) Horizons H1 and H3 are open and H2 is linked along a slip-aligned branch lines (bold). A through-going fault connects the HWF and FWF on H2 with a relict fault tip (dark grey) along-strike of HWF. Arrows indicate the proportion of slip taken up on different sections of the overlapping faults. Fault movement on the HWF is partially restricted due to the bypass of deformation from the relict fault tip onto the through-going fault, H2. To maintain strain compatibility between horizons restricted movement on the relict fault at H2 is communicated up and down dip onto H1 and H3. Likewise, movement on the HWF on H1 and H3 will be communicated onto the relict fault tip. (b) d-x profiles for H2, displacement drops across the branch lines. (c) The d-x profiles on H1 and H3, for the HWF (dashed line).

References

Amato, A., Azzara, R., Chiarabba, C., Cimini, G.B., Cocco, M., Di Bona, M., Margheriti, L., Mazza, S., Mele, F., Selvaggi, G., Basili, A., Boschi, E., Courboulex, F., Deschamps, A.,

500 Gaffet, S., Bittarelli, G., Chiaraluce, L., Piccinini, D., Ripepe, M., 1998. The 1997
501 Umbria-Marche, Italy, Earthquake Sequence: A first look at the main shocks and
502 aftershocks. Geophys. Res. Lett. 25 (15), 2861-2864.
503 Bonson, C.G., Childs, C., Walsh, J.J., Schopfer, M.P.J., Carboni, V., 2007. Geometric and
504 kinematic controls on the internal structure of a large normal fault in massive
505 limestones; the Maghlaq Fault, Malta. Journal of Structural Geology 29 (2), 336-354.
506 Childs, C., Watterson, J., Walsh, J.J., 1995. Fault overlap zones within developing normal
507 fault systems. Journal of the Geological Society of London 152 (3), 535-549.
508 Childs, C., Watterson, J., Walsh, J.J., 1996. A model for the structure and development of
509 fault zones. Journal of the Geological Society of London 153 (3), 337-340.
510 Crider, J.G., Peacock, D.C.P., 2004. Initiation of brittle faults in the upper crust: a review of
511 field observations. Journal of Structural Geology 26 (4), 691-707.
512 Davatzes, N.C., Eichhubl, P., Aydin, A., 2005. Structural evolution of fault zones in sandstone
513 by multiple deformation mechanisms: Moab fault, southeast Utah. Geological
514 Society of America Bulletin 117 (1-2), 135-148.
515 De Ruig, M., Trupp, M., Bishop, D., Kuek, D., Castillo, D., 2000. Fault architecture and the
516 mechanics of fault reactivation in the Nancar Trough/Laminaria area of the Timor
517 Sea, northern Australia. APPEA Journal 40174–193.
518 Ferrill, D.A., Morris, A.P., 2003. Dilational normal faults. Journal of Structural Geology 25 (2),
519 183-196.
520 Ferrill, D.A., Stamatakos, J.A., Sims, D., 1999. Normal fault corrugation: implications for
521 growth and seismicity of active normal faults. Journal of Structural Geology 21 (8-9),
522 1027-1038.
523 Huggins, P., Watterson, J., Walsh, J.J., Childs, C., 1995. Relay zone geometry and
524 displacement transfer between normal faults recorded in coal-mine plans. Journal of
525 Structural Geology 17 (12), 1741-1755.
526 Imber, J., Tuckwell, G.W., Childs, C., Walsh, J.J., Manzocchi, T., Heath, A.E., Bonson, C.G.,
527 Strand, J., 2004. Three-dimensional distinct element modelling of relay growth and
528 breaching along normal faults. Journal of Structural Geology 26 (10), 1897-1911.
529 Kristensen, M.B., Childs, C.J., Korstgård, J.A., 2008. The 3D geometry of small-scale relay
530 zones between normal faults in soft sediments. Journal of Structural Geology 30 (2),
531 257-272.
532 Long, J.J., 2011. Geometry, evolution and scaling of fault relay zones in 3D using detailed
533 observations from outcrops and 3D seismic data. Ph.D. Thesis, Durham University.
534 Long, J.J., Imber, J., 2010. Geometrically coherent continuous deformation in the volume
535 surrounding a seismically imaged normal fault-array. Journal of Structural Geology
536 32 (2), 222-234.
537 Machette, M.N., Personius, S.F., Nelson, A.R., Schwartz, D.P., Lund, W.R., 1991. The Wasatch
538 fault zone, utah--segmentation and history of Holocene earthquakes. Journal of
539 Structural Geology 13 (2), 137-149.
540 Maerten, L., Willemse, E.J.M., Pollard, D.D., Rawnsley, K., 1999. Slip distributions on
541 intersecting normal faults. Journal of Structural Geology 21 (3), 259-272.
542 McGrath, A.G., Davison, I., 1995. Damage zone geometry around fault tips. Journal of
543 Structural Geology 17 (7), 1011-1024.
544 Peacock, D.C.P., Sanderson, D.J., 1991. Displacements, segment linkage and relay ramps in
545 normal fault zones. Journal of Structural Geology 13 (6), 721-733.

546 Peacock, D.C.P., Sanderson, D.J., 1992. Effects of layering and anisotropy on fault geometry.
547 Journal of the Geological Society 149 (5), 793-802.
548 Peacock, D.C.P., Sanderson, D.J., 1994. Geometry and development of relay ramps in normal
549 fault systems. AAPG Bulletin 78 (2), 147-165.
550 Pedersen, S., Skov, T., Randen, T., Sønneland, L., 2005. Automatic Fault Extraction Using
551 Artificial Ants, In: Iske, A., Randen, T. (Eds.), Mathematical Methods and Modelling in
552 Hydrocarbon Exploration and Production. Springer Berlin Heidelberg, pp. 107-116.
553 Schöpfer, M.P.J., Childs, C., Walsh, J.J., 2006. Localisation of normal faults in multilayer
554 sequences. Journal of Structural Geology 28 (5), 816-833.
555 Schwartz, D.P., Coppersmith, K.J., 1984. Fault Behavior and Characteristic Earthquakes:
556 Examples From the Wasatch and San Andreas Fault Zones. J. Geophys. Res. 89 (B7),
557 5681-5698.
558 Sieh, K., Jones, L., Hauksson, E., Hudnut, K., Eberhart-Phillips, D., Heaton, T., Hough, S.,
559 Hutton, K., Kanamori, H., Lilje, A., Lindvall, S., McGill, S.F., Mori, J., Rubin, C., Spotila,
560 J.A., Stock, J., Thio, H.K., Treiman, J., Wernicke, B., Zachariasen, J., 1993. Near-Field
561 Investigations of the Landers Earthquake Sequence, April to July 1992. Science 260
562 (5105), 171-176.
563 Soliva, R., Benedicto, A., Schultz, R.A., Maerten, L., Micarelli, L., 2008. Displacement and
564 interaction of normal fault segments branched at depth: Implications for fault
565 growth and potential earthquake rupture size. Journal of Structural Geology 30 (10),
566 1288-1299.
567 Walsh, J.J., Bailey, W.R., Childs, C., Nicol, A., Bonson, C.G., 2003. Formation of segmented
568 normal faults; a 3-D perspective. Journal of Structural Geology 25 (8), 1251-1262.
569 Walsh, J.J., Watterson, J., 1991. Geometric and kinematic coherence and scale effects in
570 normal fault systems, In: Roberts, A.M., Yielding, G., Freeman, B. (Eds.), The
571 geometry of normal faults. Geological Society, London, Special Publications, pp. 193-
572 203.
573 Walsh, J.J., Watterson, J., Bailey, W.R., Childs, C., 1999. Fault relays, bends and branch-lines.
574 Journal of Structural Geology 21 (8-9), 1019-1026.
575 Wesnousky, S.G., 1986. Earthquakes, Quaternary Faults, and Seismic Hazard in California. J.
576 Geophys. Res. 91 (B12), 12587-12631.
577 Whittam, D.B., Norvick, M.S., McIntyre, C.L., 1996. Mesozoic and Cainozoic
578 tectonostratigraphy of western ZOCA and adjacent areas. APPEA Journal 36 (1), 209-
579 231.
580 Wyrick, D.Y., Morris, A.P., Ferrill, D.A., 2011. Normal fault growth in analog models and on
581 Mars. Icarus 212 (2), 559-567.
582
583

Figure 1

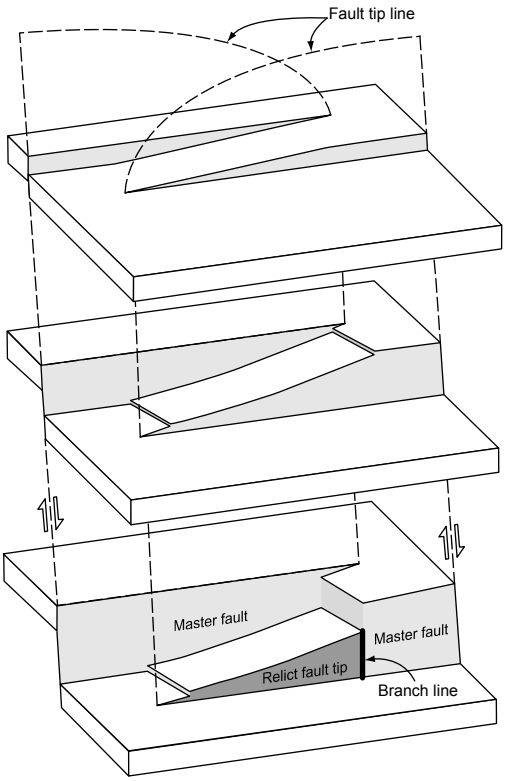
Fault tip line
Master fault
Master fault
Relict fault tip
Branch line

Figure 2

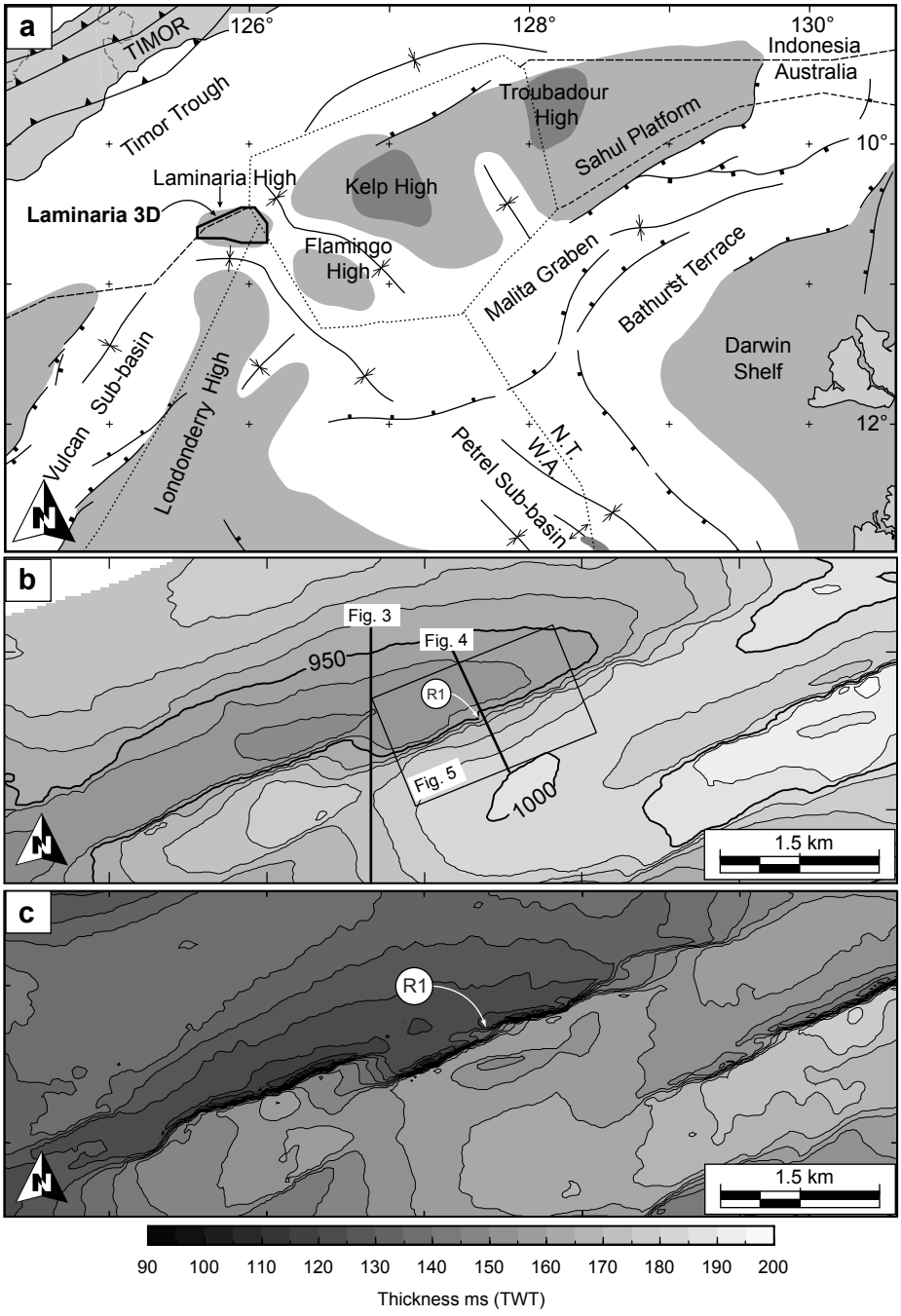
a
TIMOR
126°
128°
130°
Indonesia
Australia
Timor Trough
Troubadour High
Sahul Platform
10°
Laminaria High
Kelp High
Laminaria 3D
Flamingo High
Malita Graben
Bathurst Terrace
Darwin Shelf
Vulcan Sub-basin
Londonderry High
N.T.
W.A
Petrel Sub-basin
12°
b
Fig. 3
Fig. 4
950
R1
Fig. 5
1000
1.5 km
c
R1
1.5 km
90 100 110 120 130 140 150 160 170 180 190 200
Thickness ms (TWT)

Figure 3

Click here to download high resolution image

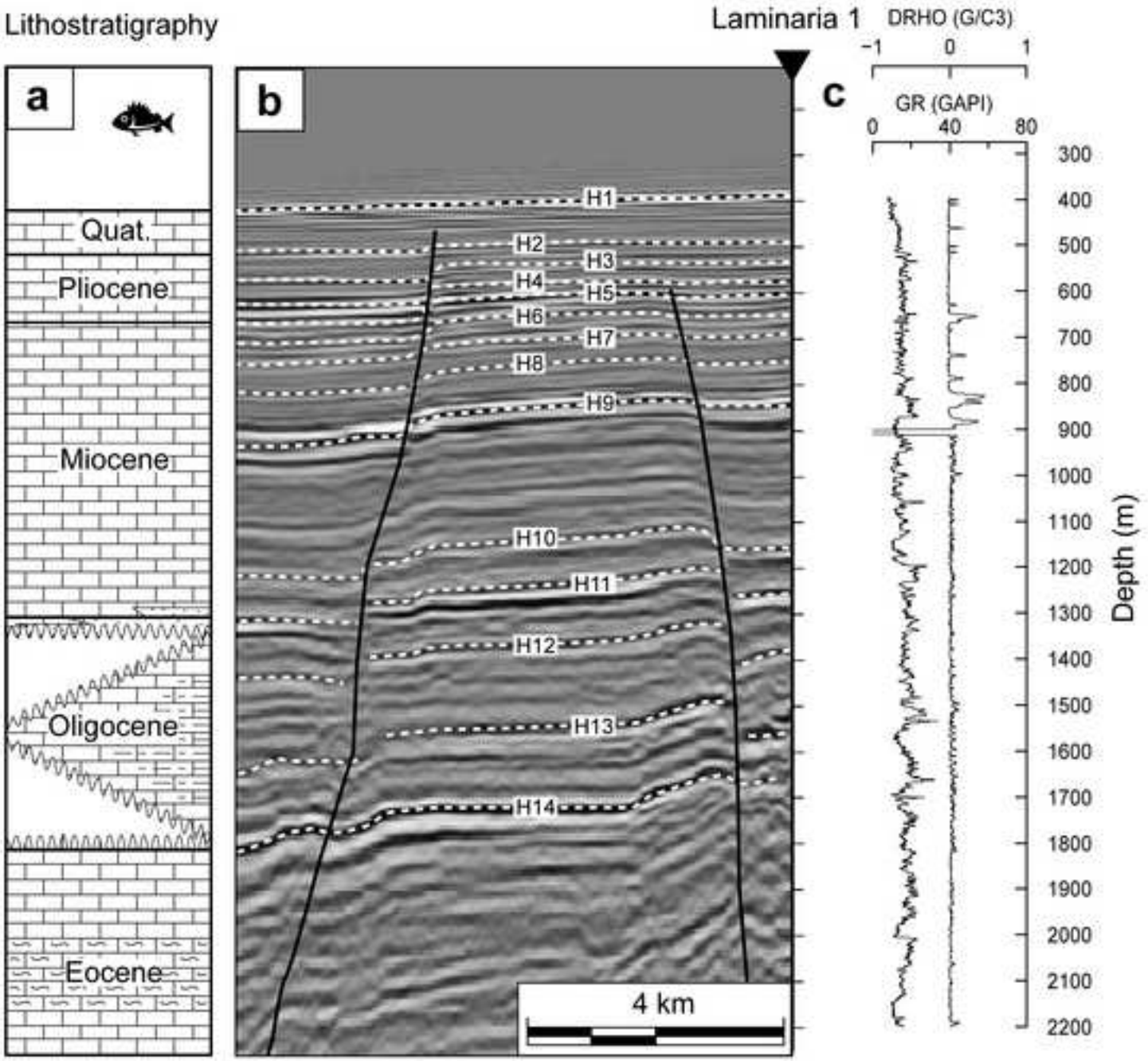

Figure 4

Click here to download high resolution image

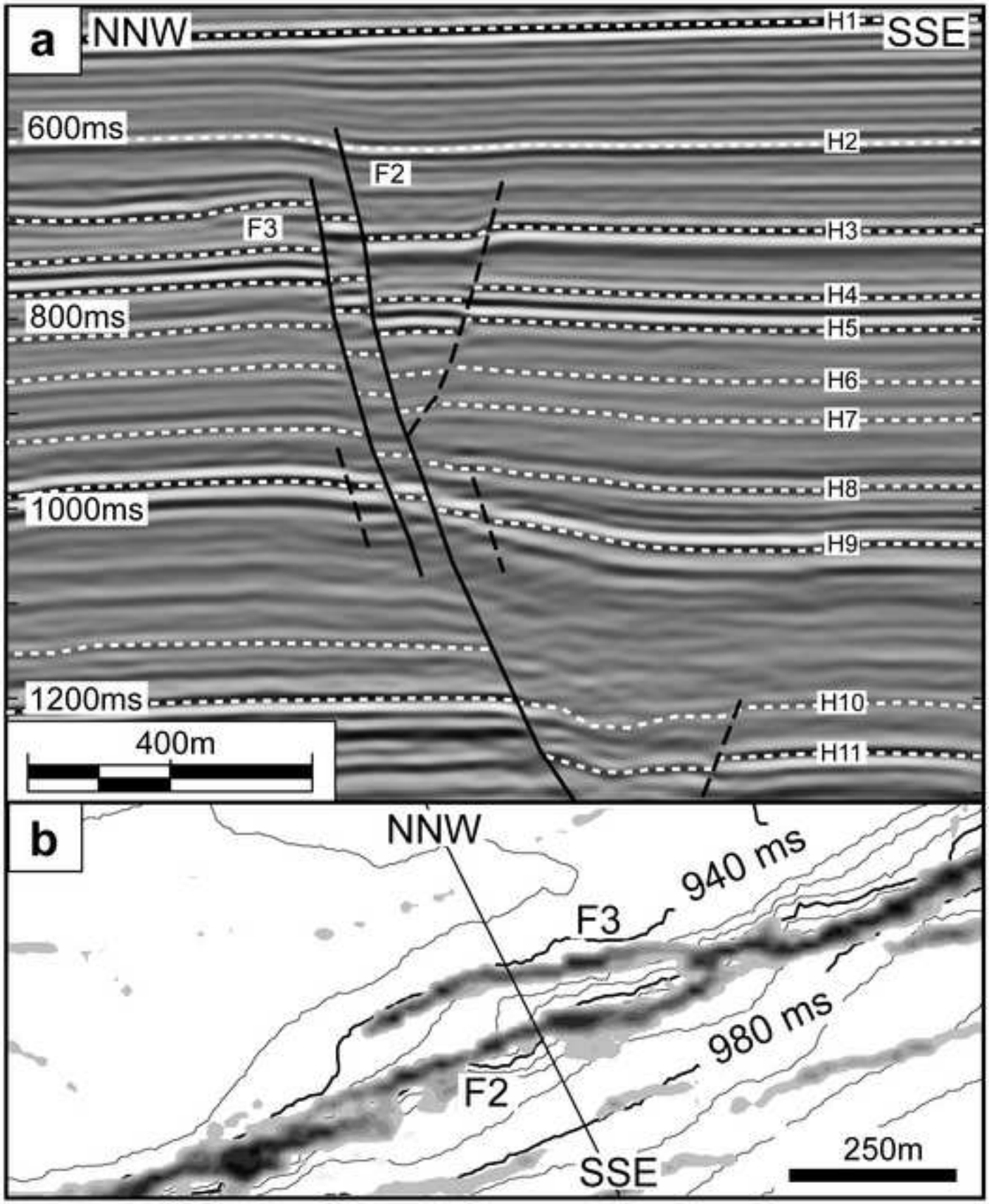

Figure 5

Click here to download high resolution image

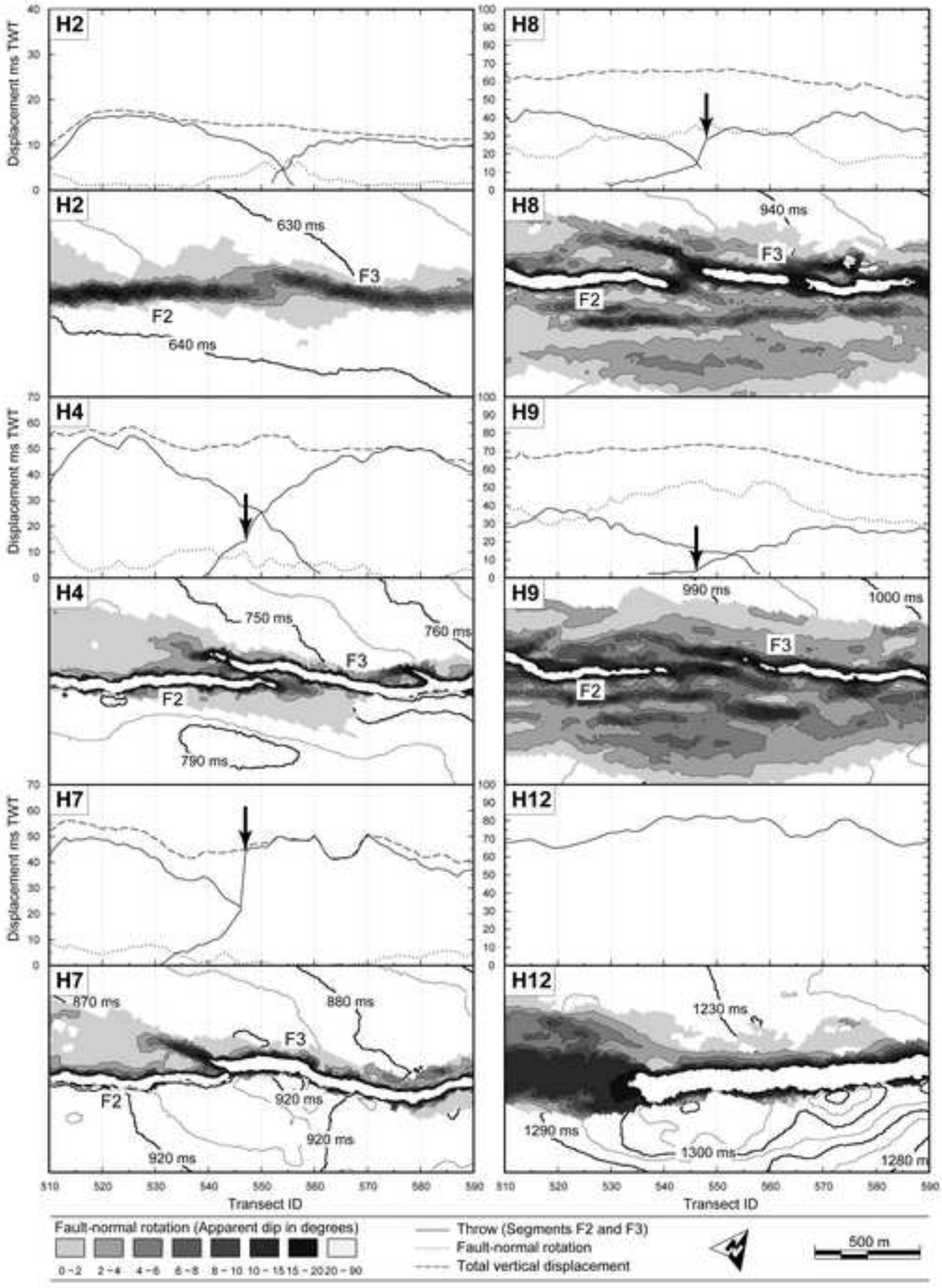

Figure 6

Click here to download high resolution image

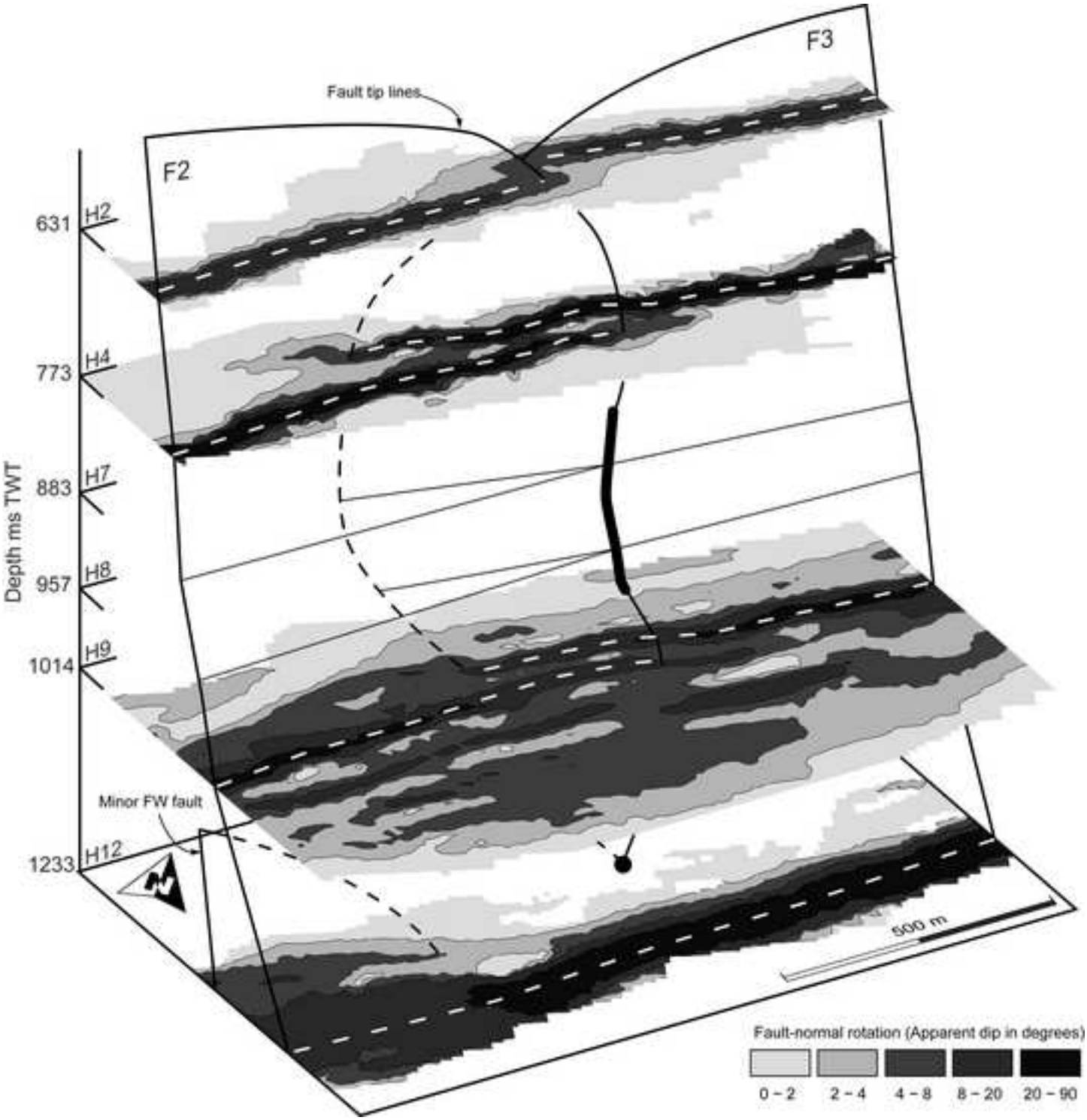

Figure 7 colour version for online

Click here to download high resolution image

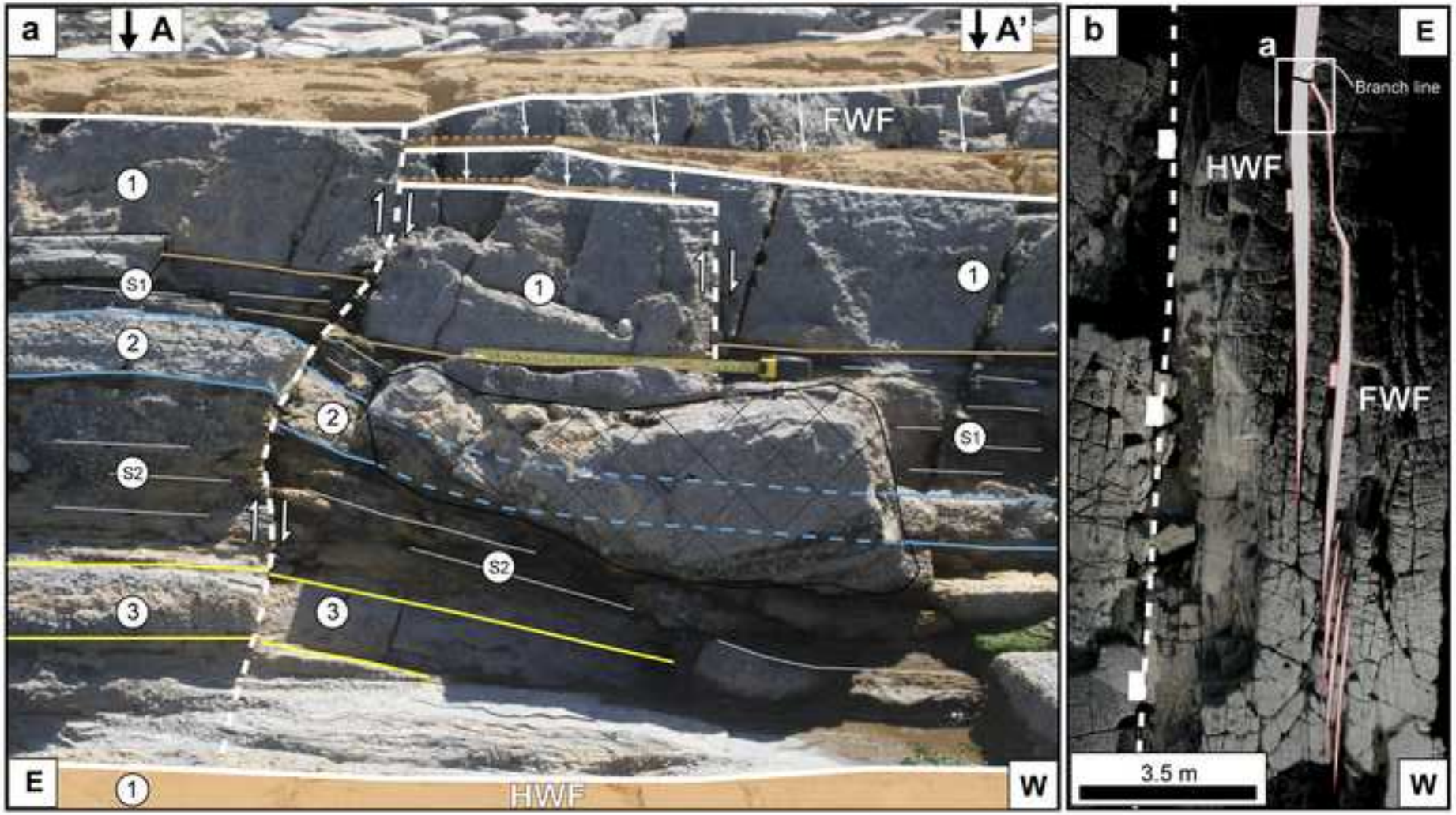

Figure 7 B&W version for print

Click here to download high resolution image

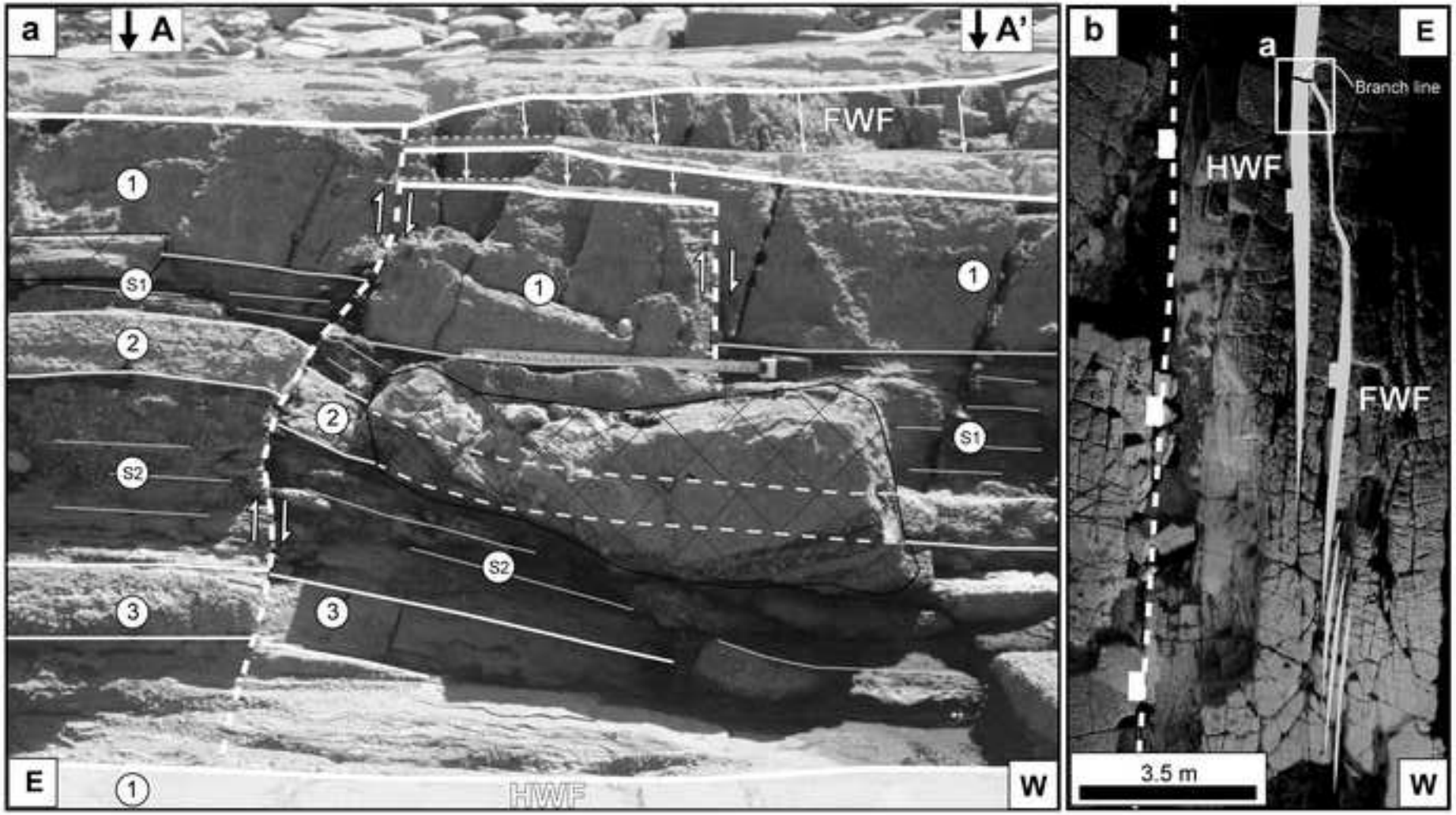

Figure 8

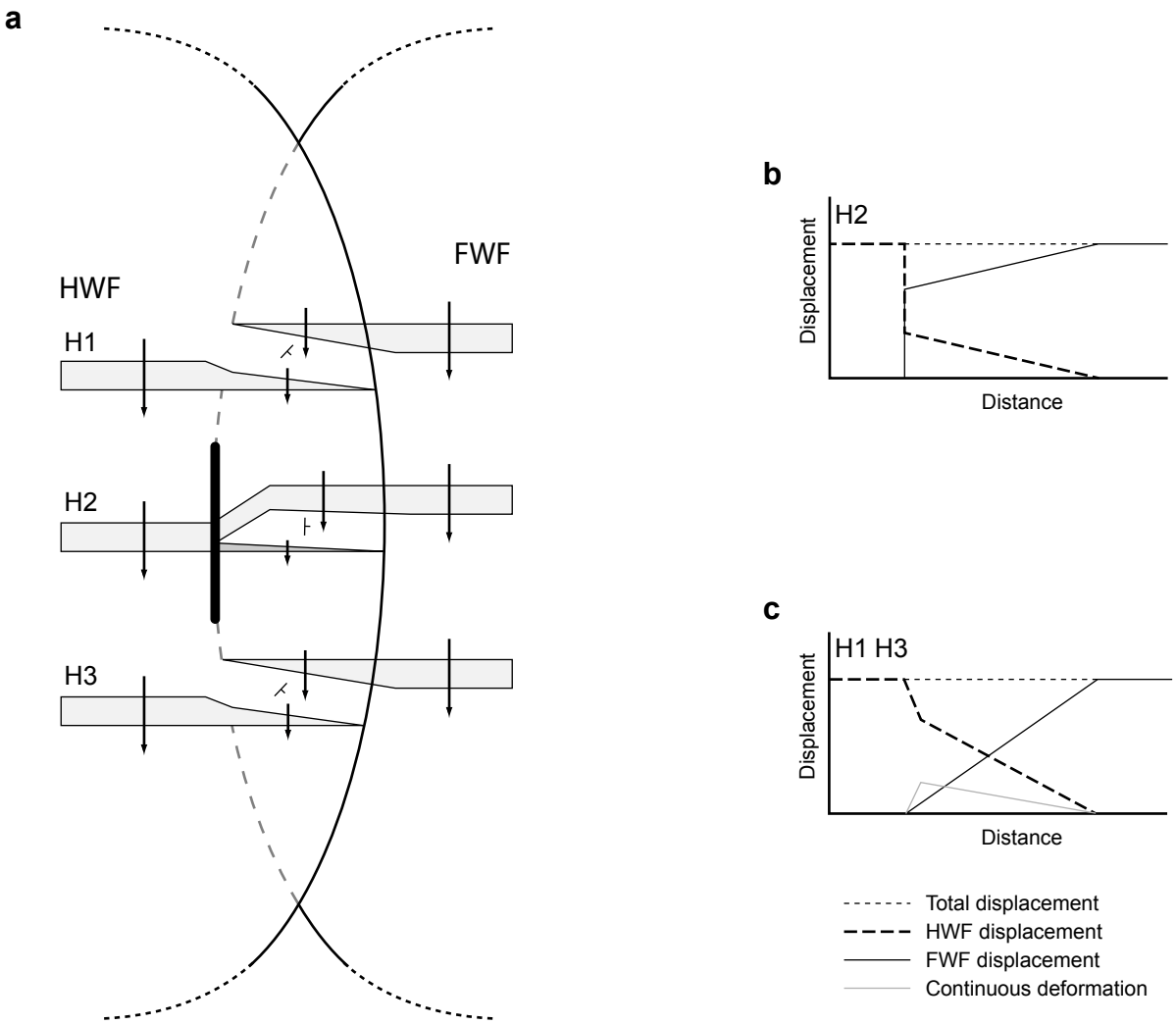
a
HWF
FWF
H1
H2
H3
b
H2
Displacement
Distance
c
H1 H3
Displacement
Distance
Total displacement
HWF displacement
FWF displacement
Continuous deformation